Jurnal Polimesin
Department of Mechanical Engineering
State Polytechnic of Lhokseumawe
http://e-jurnal.pnl.ac.id/polimesin
e-ISSN : 2549-1999 No. : 6 Month : December
p-ISSN : 1693-5462 Volume : 23 Year : 2025

Processing dates: received on 2025-10-30, reviewed on 2025-12-17, accepted on 2025-12-22 and online availability on 2025-12-31

Experimental optimization of welding current, strip thickness, and spot number for the mechanical integrity of 18650 lithium-ion battery pack joints

Arman*, Widya Jufri, Baso Nasrullah
Department of Mechanical Engineering, Politeknik Negeri Ujung Pandang, Makassar 90245, Indonesia
*Corresponding author: arman@poliupg.ac.id

Abstract

The accelerating transition to renewable energy has driven widespread use of 18650 lithium-ion cells in electric vehicles and portable electronics, making the integrity of resistance spot-welded joints critical for system safety and reliability. This study investigates the effects of material thickness, number of weld points, and welding current on the mechanical performance of spot-welded joints. SPCC nickel strips with thicknesses of 0.10 mm, 0.12 mm, and 0.15 mm were welded to 18650 cells using a CNC-controlled spot-welding machine in three operating modes (7, 8, and 9). The mechanical performance was assessed through shear and peel force tests. The results showed that the welding current and the number of weld points had a dominant influence on the joint load-bearing capacity. Six weld points consistently improved load distribution, while material thickness significantly improved performance, with a 0.15 mm strip producing the highest shear force of 2380 N and a peel force of 2400 N. Optimal performance was achieved at 25 A (Mode 9), where failure occurred primarily in the base metal, indicating a strong metallurgical bond. SEM analysis shows the 0.12 mm thickness produces more homogeneous surfaces with fewer micro-cracks. The results reveal a trade-off between performance metrics, where 0.15 mm achieves higher load-bearing capacity, whereas 0.12 mm offers improved microstructural stability and long-term reliability. Optimizing spot welding parameters is essential for achieving reliable battery interconnections, as increasing the number of weld points enhances mechanical robustness while appropriate current levels improve joint integrity without inducing thermal damage.

Keywords:
18650 lithium-ion battery, spot welding, shear force, peel force.

1 Introduction

The global transition to renewable energy has driven rapid developments in battery technology, particularly the 18650 lithium-ion batteries. This type of battery is an essential component in a wide range of applications, from electric vehicles to portable electronic devices due to its high energy density[1]. Typically, a standard automotive battery pack consists of hundreds, even thousands, of individual lithium-ion cells that are connected in series or parallel in order to achieve the required power and energy [2].

In the battery pack assembly process, one of the most critical steps is the connection of the batteries with tabs. This step is crucial for the performance, efficiency, and lifespan of the battery. Various joining methods have been studied, such as ultrasonic welding, laser welding, soldering, and resistance spot welding. Among these methods, resistance spot welding is considered one of the most widely used methods in the industry due to its versatility, cost-effectiveness, and ability to produce strong joints on various types of battery cells, including 18650 cylindrical batteries [3]. In general, Resistance Spot Welding (RSW) is effective because the joining process is controlled by the electrical current passing through the contact interfaces. The process operates on the principle of electrical resistance mating surfaces, which generates localized heating and material fusion under pressure when a high current passes through them. Furthermore, RSW is particularly well suited for joining nickel-based tabs to cylindrical lithium-ion cells [4].

Resistance spot welding is a metal interface welding process that forms a molten joint (nugget) without the need for additional material [5]. This method is capable of producing joints that are not only mechanically strong but also have low contact resistance, an important parameter for the electrical efficiency and thermal management of the battery [6]. In automotive and related industries, component geometry optimization and weight reduction are key design considerations, further promoting the widespread use of resistance spot welding. However, lightweight design must not compromise joint reliability and structural strength. Resistance spot welding is a filler-free joining process in which electrodes with high electrical and thermal conductivity clamp the sheets and apply high current to generate localized heating and form a weld nugget. The high temperatures reached during this process, often close to the melting point, can alter the metallurgical structure of the materials, thereby affecting mechanical properties such as tensile strength, corrosion resistance, and surface hardness. Consequently, mechanical evaluation of spot-welded joints is essential to ensure joint integrity [7].

Despite its widespread use, the application of RSW in lithium - ion batteries faces complex challenges. The main challenge is preventing thermal damage to the sensitive battery cells. Improper parameter control can lead to overheating that damages the cell's internal components, potentially triggering short circuits and thermal runaway [8]. In addition, the joint quality is greatly influenced by various process and material factors, such as welding current, strip thickness, and the number of weld points. Therefore, thorough evaluation through mechanical testing, such as shear and peel tests, is crucial to validate the joint integrity [9].

Several previous studies have highlighted the importance of parameter optimization. A study by Bauman *et al.* [11] showed that proper parameter settings can significantly improve the shear strength and reduce the contact resistance in cylindrical battery joints. Another study by Bieliszczuk and Zyskowska revealed that the joint strength of single-sided 18650 battery tabs varies significantly depending on the preparation conditions and welding parameters [10]. These findings emphasize that the investigation of process parameters is a crucial step to ensure joint quality. Based on this background and a review of recent developments, the present study focuses on the investigation of the joint strength of spot welds in 18650 lithium-ion battery packs.

Various welding techniques have been developed to improve joint strength and manufacturing efficiency, with RSW remaining the most widely applied method for cylindrical lithium-ion 18650 battery pack assembly [12]. Previous studies emphasize that welding parameter control plays a critical role in achieving strong and reliable joints. Mechanical characterization, including strength evaluation and microstructural observation, is essential for understanding joint integrity and failure behavior in welded connections [13]. In this study, optimization is defined as an experimental and comparative approach to identify the most favorable combination of RSW parameters based on mechanical performance and microstructural responses, rather than the use of a statistical optimization model.

Although numerous studies have investigated resistance spot welding parameters for battery applications, most focus on single-variable optimization or electrical performance. Comprehensive experimental evaluation integrating welding current, strip

thickness, and number of weld points, particularly linked to failure modes and microstructural evolution in 18650 battery packs, remains limited. This study aims to address the existing research gap.

2 Research methodology

This study used 18650 lithium-ion batteries (Ø18 mm × 65 mm, 3.7 V) and SPCC nickel strips with thicknesses of 0.10 mm, 0.12 mm, and 0.15 mm (width 6 mm), which were purchased from an online electronics supplier. The equipment included a 3-axis CNC spot welding machine, a Galdabini FM.100 Universal Testing Machine (UTM), a special peel force tester equipped with a force gauge, an AFFRI system hardness tester (model OMAG G-6AS, Italy) and a FlexSEM 1000 II Scanning Electron Microscope.

2.1 Welding process

The spot welding process was carried out using a 3-axis CNC spot welding machine. SPCC nickel strips, each 100 mm long, were welded in modes 7, 8, and 9, which correspond to increasing welding current levels (approximately 23–26 A) with fixed electrode geometry and pressure settings, as predefined by the CNC spot welding system.

2.2 Mechanical testing

The mechanical performance of the welded joints was assessed through shear and peel force tests. Shear force measurements were carried out using a Galdabini FM.100 UTM, while peel force tests were conducted with a custom-designed fixture equipped with a digital force gauge to record the maximum load at failure. Each test configuration was repeated three times to ensure data reliability and reproducibility. The fracture locations were visually examined and documented to determine the dominant failure mode—whether it occurred within the weld metal and base metal.

2.3 Hardness testing

The Vickers micro-hardness test was conducted on three key regions: the nugget, the Heat-Affected Zone (HAZ), and the base material. Three readings were taken from each region, and the average value was calculated.

2.4 SEM and EDS testing

The surface morphology and elemental composition of the weld joints, encompassing the nugget zone, the HAZ, and base metal, were analyzed using Scanning Electron Microscopy (SEM) and Energy Dispersive Spectroscopy (EDS). This analysis aimed to evaluate fusion quality, detect defects, and investigate elemental diffusion in samples with varying thicknesses (0.10 mm, 0.12 mm, and 0.15 mm), each featuring six weld points.

3 Results and discussion

3.1 Shear and peel force testing

To evaluate the mechanical performance of spot-welded joints, shear force tests were performed on samples with variations in material thickness, number of weld points, and welding modes. The outcomes of these experiments are summarized in Table 1–Table 3, which display the corresponding shear force and fracture locations for each configuration. In addition, Fig. 1–Fig. 3 are provided to illustrate the comparative effects of thickness, weld points, and welding current on joint behavior. All tests were repeated three times, and results are presented as mean ± standard deviation.

Table 1. Shear force of spot welding Mode 7

Sample code	Size thickness × width	Spot welding	Current	Shear force	± SD	Fracture location
	mm	Points	Ampere	N	N	
M7T1S2	0.10 × 6	2	24.4	2220	±48	Weld metal
M7T1S4	0.10 × 6	4	24.0	2250	±52	Weld metal
M7T1S6	0.10 × 6	6	23.9	2300	±50	Base metal
M7T12S2	0.12 × 6	2	22.9	2200	±44	Weld metal
M7T12S4	0.12 × 6	4	21.0	2240	±47	Weld metal
M7T12S6	0.12 × 6	6	25.0	2310	±53	Base metal
M7T15S2	0.15 × 6	2	18.2	2220	±45	Weld metal
M7T15S4	0.15 × 6	4	23.4	2260	±49	Weld metal
M7T15S6	0.15 × 6	6	22.6	2320	±53	Weld metal

Table 2. Shear force of spot welding Mode 8

Sample code	Size thickness × width	Spot welding	Current	Shear force	± SD	Fracture location
	mm	Points	Ampere	N	N	
M8T1S2	0.10 × 6	2	24.2	2260	±38	Weld metal
M8T1S4	0.10 × 6	4	25.8	2290	±42	Weld metal
M8T1S6	0.10 × 6	6	25.6	2310	±40	Base metal
M8T12S2	0.12 × 6	2	24.7	2260	±35	Weld metal
M8T12S4	0.12 × 6	4	23.3	2280	±40	Weld metal
M8T12S6	0.12 × 6	6	24.5	2310	±45	Weld metal
M8T15S2	0.15 × 6	2	24.0	2260	±36	Weld metal
M8T15S4	0.15 × 6	4	24.2	2290	±41	Weld metal
M8T15S6	0.15 × 6	6	25.0	2330	±46	Weld metal

Table 3. Shear force of spot welding Mode 9

Sample code	Size thickness × width	Spot welding	Current	Shear force	± SD	Fracture location
	mm	Points	Ampere	N	N	
M9T1S2	0.10 × 6	2	24.8	2300	±32	Weld metal
M9T1S4	0.10 × 6	4	25.7	2330	±36	Weld metal
M9T1S6	0.10 × 6	6	25.9	2350	±38	Base metal
M9T12S2	0.12 × 6	2	25.5	2300	±30	Weld metal
M9T12S4	0.12 × 6	4	24.9	2320	±34	Weld metal
M9T12S6	0.12 × 6	6	24.2	2360	±40	Base metal
M9T15S2	0.15 × 6	2	25.7	2310	±31	Weld metal
M9T15S4	0.15 × 6	4	24.4	2340	±35	Weld metal
M9T15S6	0.15 × 6	6	25.3	2380	±42	Base metal

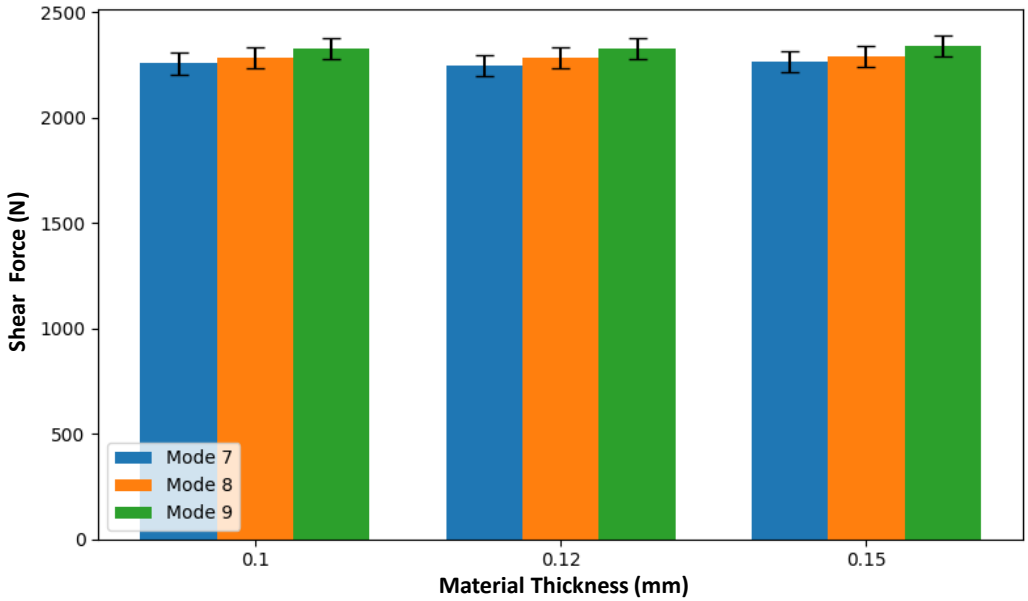

Fig. 1. Effect of material thickness on shear force.

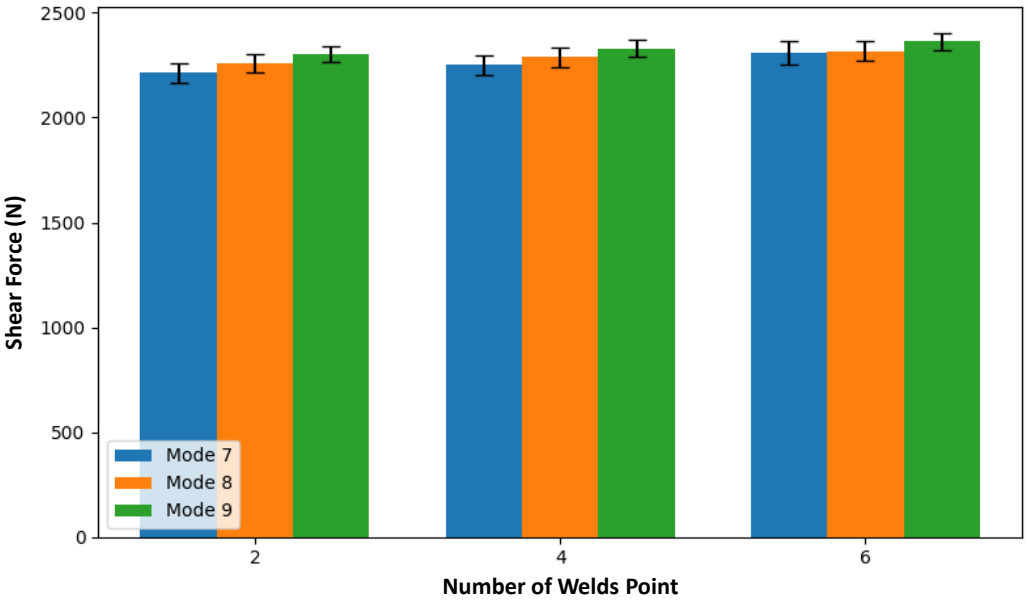

Fig. 2. Effect of number of welding points on shear force.

Fig. 3. Effect of current on shear force.

Based on Table 1–Table 3 and Fig. 1, it can be observed that increasing the nickel strip thickness from 0.10 mm to 0.15 mm does not result in a significant improvement in shear force. Higher welding currents promote larger nugget formation due to increased heat input at the faying interface between the nickel strip and battery tab. The enlargement of the nugget area enhances the effective load-bearing cross-section, resulting in higher shear and peel forces. As the nugget size increases and metallurgical bonding becomes more complete, the dominant failure mode shifts from weld metal failure to base metal failure, particularly at higher current levels (Mode 9). This transition indicates sufficient fusion and favorable heat distribution during the welding process, which is consistent with the observed increase in hardness values in the HAZ. The shear force values tend to remain stable within the range of 2200–2320 N. This indicates that, within the tested range, the material thickness is not the dominant factor affecting the shear force. Fig. 2, it can be seen that the number of weld spots has a more pronounced effect. Each additional weld spot (from 2 to 6) tends to increase the shear force. For example, in Mode 9 with a thickness of 0.15 mm, the shear force increased from 2250 N (2 spots) to 2320 N (6 spots). This demonstrates that a higher number of weld spots distributes the load more evenly, thereby enhancing joint load-bearing capacity. Fig. 3 illustrates the dominant influence of welding current on shear force. Higher currents (around 25 A) tend to produce better shear force, consistent with previous parametric studies on resistance spot welding of lithium-ion battery tabs, which reported that increased welding current promotes larger nugget formation and stronger metallurgical bonding [1] [4], [5].

The peel force values presented in Table 4–Table 6 were obtained from peel tests conducted using a universal testing machine, representing the global peel strength of the welded joints. Based on Table 4–Table 6 and Fig. 4, the material thickness exhibits a more pronounced effect on the peel test compared to the shear test. A strip thickness of 0.15 mm yielded the highest peel force values, reaching up to 2400 N in Mode 9. Fig. 5 show that effect of the number of weld points on peel force indicates that the number of weld spots also has a positive influence on peel force. An increase in the number of weld spots corresponds to a greater joint capacity to withstand peel loads. However, similar to the shear test, the improvement is not always linear and may be affected by the consistency of the welding process. Fig. 6 illustrates the effect of current on peel force, it can be observed that higher welding currents tend to enhance peel force. A current of approximately 25 A in Mode 9 results in peel force values of up to 2400 N. The observed trend aligns with previous studies on resistance spot welding of lithium-ion battery tabs, which reported that higher welding currents and sufficient heat input improve nugget integrity and peel resistance [4], [8].

Table 4. Peel force of spot welding Mode 7

Sample code	Size thickness × width	Spot welding	Current	Shear force	± SD	Fracture location
	mm	Points	Ampere	N	N	
M7K1S2	0.10 × 6	2	24.4	2180	±48	Weld metal
M7K1S4	0.10 × 6	4	24.0	2210	±52	Weld metal
M7K1S6	0.10 × 6	6	23.9	2240	±50	Weld metal
M7K12S2	0.12 × 6	2	22.9	2200	±44	Weld metal
M7K12S4	0.12 × 6	4	21.0	2250	±48	Weld metal
M7K12S6	0.12 × 6	6	25.0	2280	±53	Weld metal
M7K15S2	0.15 × 6	2	18.2	2220	±45	Weld metal
M7K15S4	0.15 × 6	4	23.4	2240	±49	Weld metal
M7K15S6	0.15 × 6	6	22.6	2290	±55	Weld metal

Table 5. Peel force of spot welding Mode 8

Sample code	Size thickness × width	Spot welding	Current	Shear force	± SD	Fracture location
	mm	Points	Ampere	N	N	
M8K1S2	0.10 × 6	2	24.2	2230	±42	Weld metal
M8K1S4	0.10 × 6	4	25.8	2250	±46	Weld metal
M8K1S6	0.10 × 6	6	25.6	2270	±44	Weld metal
M8K12S2	0.12 × 6	2	24.7	2240	±38	Weld metal
M8K12S4	0.12 × 6	4	23.3	2280	±42	Weld metal
M8K12S6	0.12 × 6	6	24.5	2310	±47	Weld metal
M8K15S2	0.15 × 6	2	24.0	2250	±39	Weld metal
M8K15S4	0.15 × 6	4	24.2	2290	±43	Weld metal
M8K15S6	0.15 × 6	6	25.0	2320	±48	Weld metal

Table 6. Peel force of spot welding Mode 9

Sample code	Size thickness × width	Spot welding	Current	Shear force	± SD	Fracture location
	mm	Points	Ampere	N	N	
M9K1S2	0.10 × 6	2	24.8	2280	±34	Weld metal
M9K1S4	0.10 × 6	4	25.7	2320	±38	Weld metal
M9K1S6	0.10 × 6	6	25.9	2360	±36	Weld metal
M9K12S2	0.12 × 6	2	25.5	2310	±30	Weld metal
M9K12S4	0.12 × 6	4	24.9	2340	±33	Weld metal
M9K12S6	0.12 × 6	6	24.2	2370	±39	Weld metal
M9K15S2	0.15 × 6	2	25.7	2340	±31	Weld metal
M9K15S4	0.15 × 6	4	24.4	2370	±35	Weld metal
M9K15S6	0.15 × 6	6	25.3	2400	±41	Weld metal

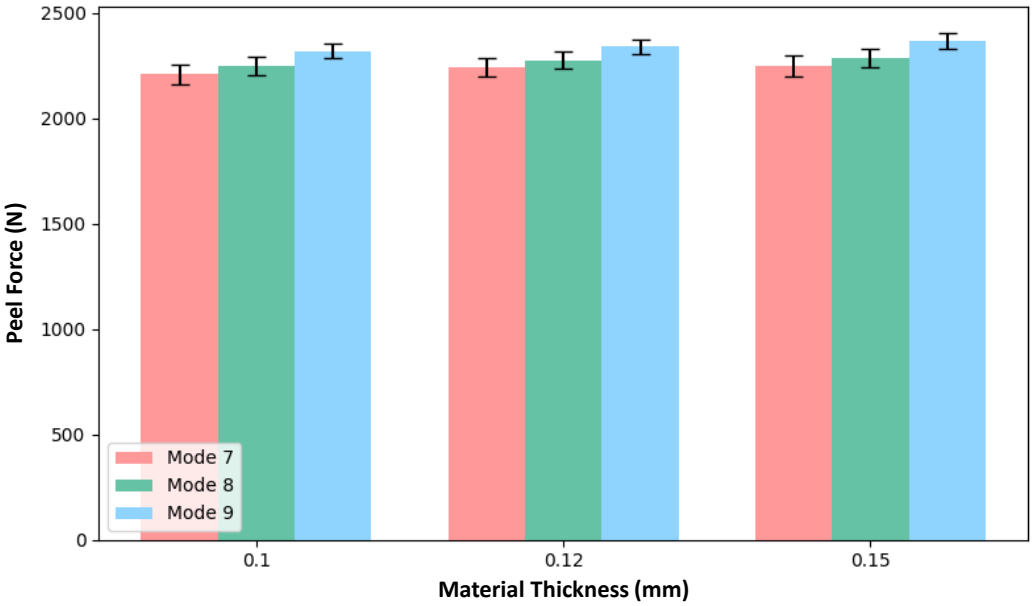

Fig. 4. Effect of material thickness on peel force.

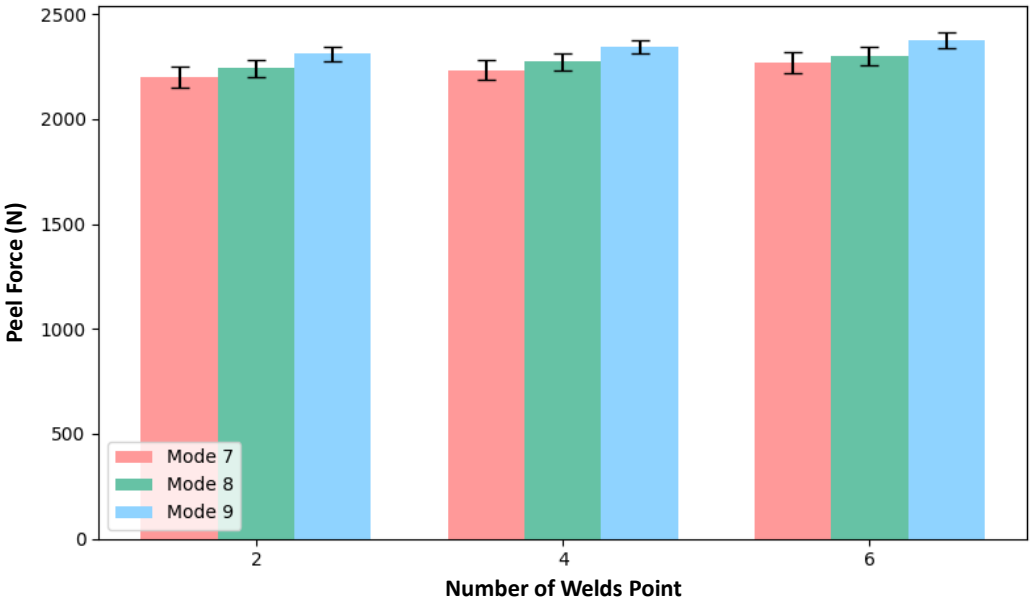

Fig. 5. Effect of number of weld points on peel force.

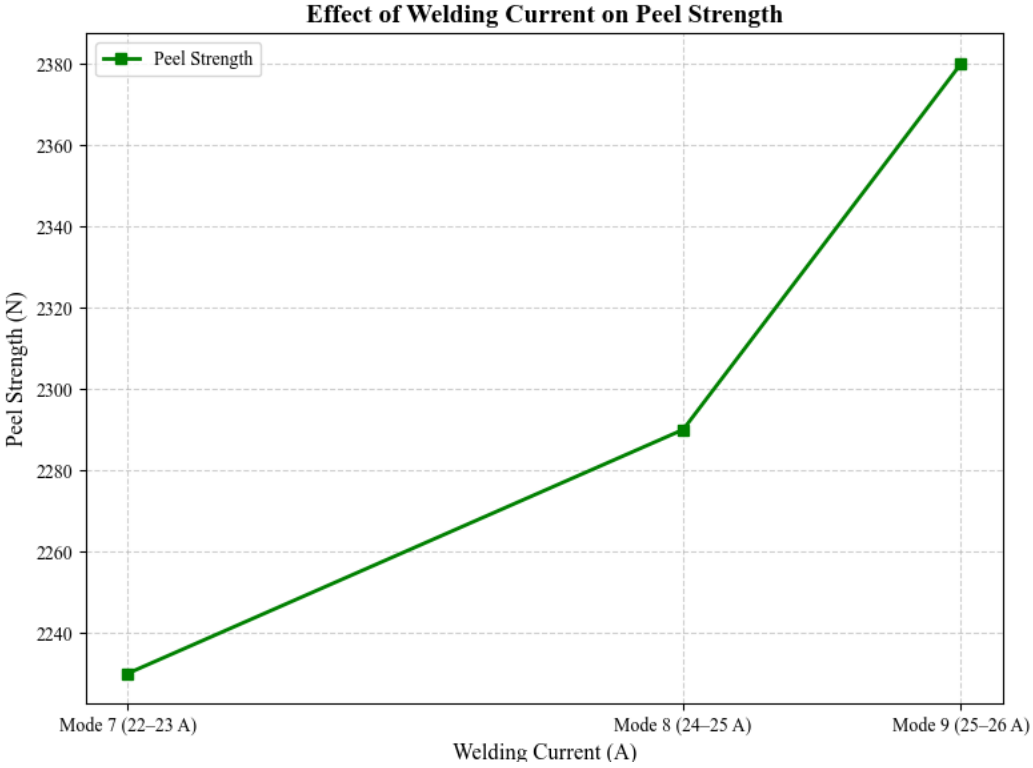

Fig. 6. Effect of current on peel force.

Based on Fig. 7, Fig. 8, and Table 7, the peel force measured using the force gauge–based tester varies with material thickness, indicating the existence of an optimal thickness that provides maximum localized peel resistance. Fig. 7 effect of material thickness on peel force shows that a thickness of 0.12 mm yields the highest peel force (193 N), whereas thicknesses of 0.10 mm and 0.15 mm exhibit lower and inconsistent values, indicating the existence of an optimal thickness for peel performance. Fig. 8 effect of the number of weld points on peel force further illustrates that increasing the number of weld spots does not always enhance load-bearing capacity; in fact, at a thickness of 0.12 mm, six weld spots provide the best performance, whereas at other thicknesses, additional weld spots reduce load-bearing capacity due to inefficient distribution of welding energy, in agreement with previous studies with previous studies on resistance spot welding of lithium-ion battery tabs, which reported that peel performance is governed by an optimal combination of material thickness and weld spot number, while excessive weld points or non-optimal thickness can lead to inefficient heat distribution and reduced load-bearing capacity [1] [4] [11].

Table 7. Peel force of spot welding Mode 9 measured using a force gauge–based peel tester

Sample code	Size thickness × width	Spot welding	Current	Shear force	± SD	Fracture location
	mm	Points	Ampere	N	N	
M9K1S2	0.10 × 6	2	73.3	47	±43	Base metal
M9K1S4	0.10 × 6	4	69.8	44	±47	Weld metal
M9K1S6	0.10 × 6	6	69.3	41	±45	Base metal
M9K12S2	0.12 × 6	2	84.8	173	±38	Base metal
M9K12S4	0.12 × 6	4	58.5	38	±42	Weld metal
M9K12S6	0.12 × 6	6	84.4	193	±48	Base metal
M9K15S2	0.15 × 6	2	28.8	64	±36	Weld metal
M9K15S4	0.15 × 6	4	46.7	37	±40	Weld metal
M9K15S6	0.15 × 6	6	58.6	46	±44	Weld metal

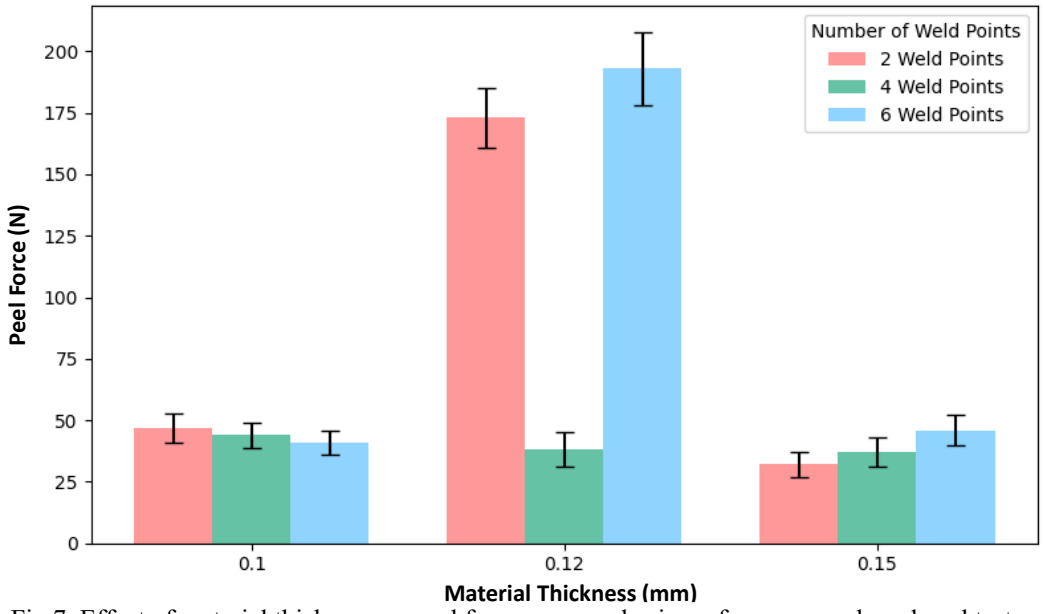

Fig 7. Effect of material thickness on peel force measured using a force gauge–based peel tester.

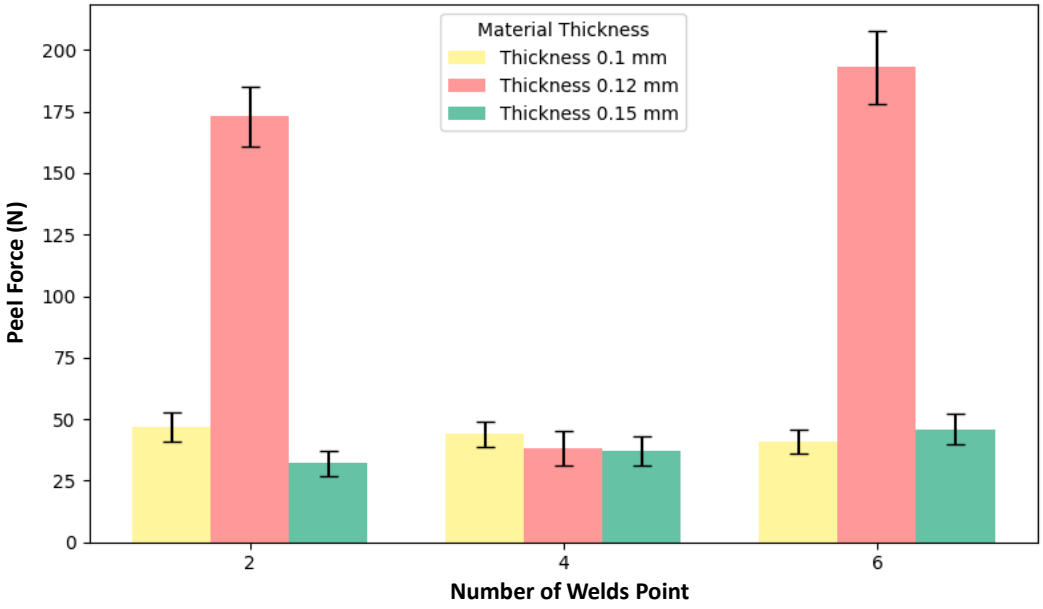

Fig. 8. Effect of number of weld points on peel force measured using a force gauge–based peel tester.

3.2 Hardness testing

To complement the mechanical performance of the load-bearing capacity of the spot welding joints, Vickers hardness tests were also conducted on samples with varying material thickness, number of weld points, and welding modes. The results of these experiments are summarized in Table 8, which displays how welding heat affects hardness in three main areas, namely the nugget, HAZ and base material. In addition, Fig. 9 and Fig. 10 are provided to illustrate the influence of material thickness and number of weld points on the Vickers hardness distribution in the nugget, HAZ, and base-material.

Table 8. Hardness test results

Sample code	Size thickness × width	Spot welding	Hardness value		
	mm	Points	Nuggets	HAZ	Base material
M9K1S2	0.10 × 6	2	52.47	58.90	54.04
M9K1S4	0.10 × 6	4	51.97	55.87	52.64
M9K1S6	0.10 × 6	6	54.00	51.97	52.00
M9K12S2	0.12 × 6	2	52.57	54.17	54.00
M9K12S4	0.12 × 6	4	47.37	48.00	57.00
M9K12S6	0.12 × 6	6	51.00	50.00	51.00
M9K15S2	0.15 × 6	2	60.57	42.00	54.00
M9K15S4	0.15 × 6	4	55.07	59.74	56.90
M9K15S6	0.15 × 6	6	55.87	63.74	59.59

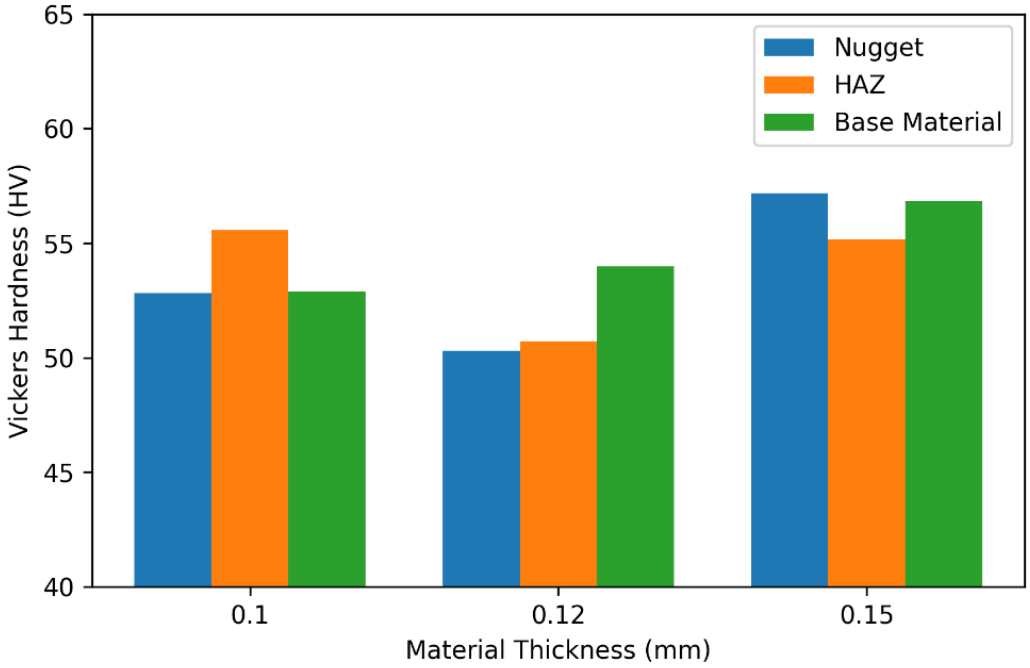

Fig. 9. Effect of material thickness on Vickers hardness in the nugget, HAZ, and base material.

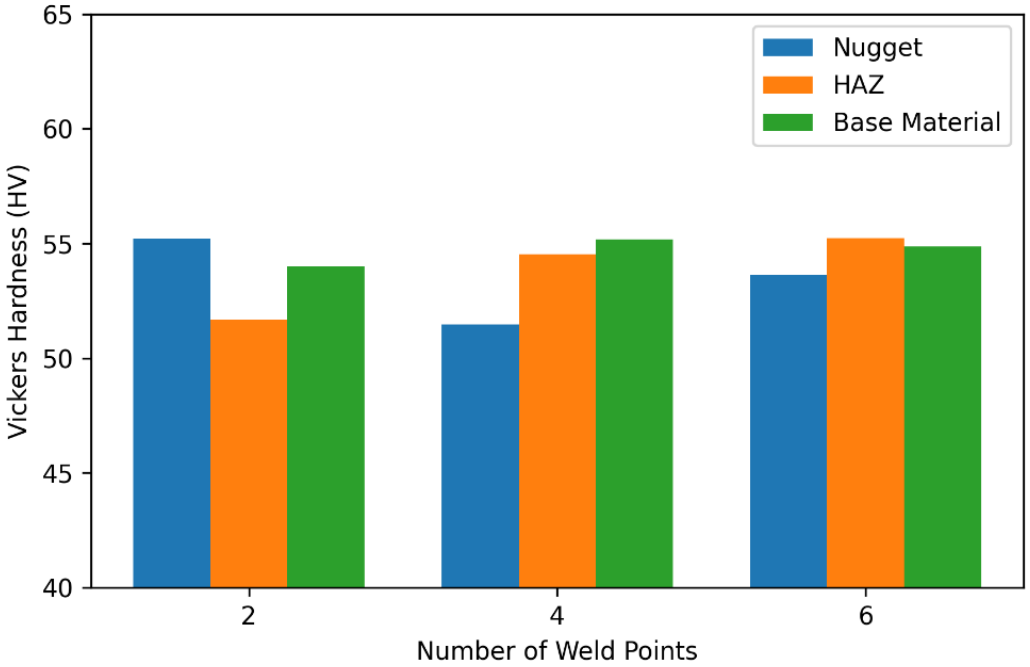

Fig. 10. Effect of number of weld points on Vickers hardness in the nugget, HAZ, and base material.

Based on Table 8 and Fig. 9-Fig. 10 it is clear that the Vickers micro-hardness distribution in the nugget, HAZ, and base material reveals the complex influence of the welding thermal cycle on the metallurgical integrity of the joint. The optimal configuration was achieved in specimen M9K15S6 (0.15 mm thickness, 6 weld points), which recorded peak hardness values of 63.74 HV in the HAZ and 59.59 HV in the base material, in accordance with previous studies on resistance spot welding of lithium-ion battery tabs, which reported that increased heat input and repeated thermal cycles promote hardness elevation in the HAZ due to microstructural refinement and localized metallurgical strengthening [5], [7], [10].

3.3 SEM and EDS testing

SEM and Energy Dispersive (EDS) testing were conducted in the laboratory of Campus 2 of Ujung Pandang State Polytechnic. SEM testing was conducted to observe the surface morphology of spot welded joints on nickel materials with a thickness of 0.10 mm, 0.12 mm and 0.15 mm and a total of 6 weld points. Observations were made at magnifications of 200×, 500×, 1000× and 3000×. The aim was to determine changes in structure and characteristics in the weld area, HAZ, and the base material. In addition, EDS can also be performed on the weld area to determine the elemental composition found on the metal surface. The results of the SEM testing can be seen in Fig. 11.

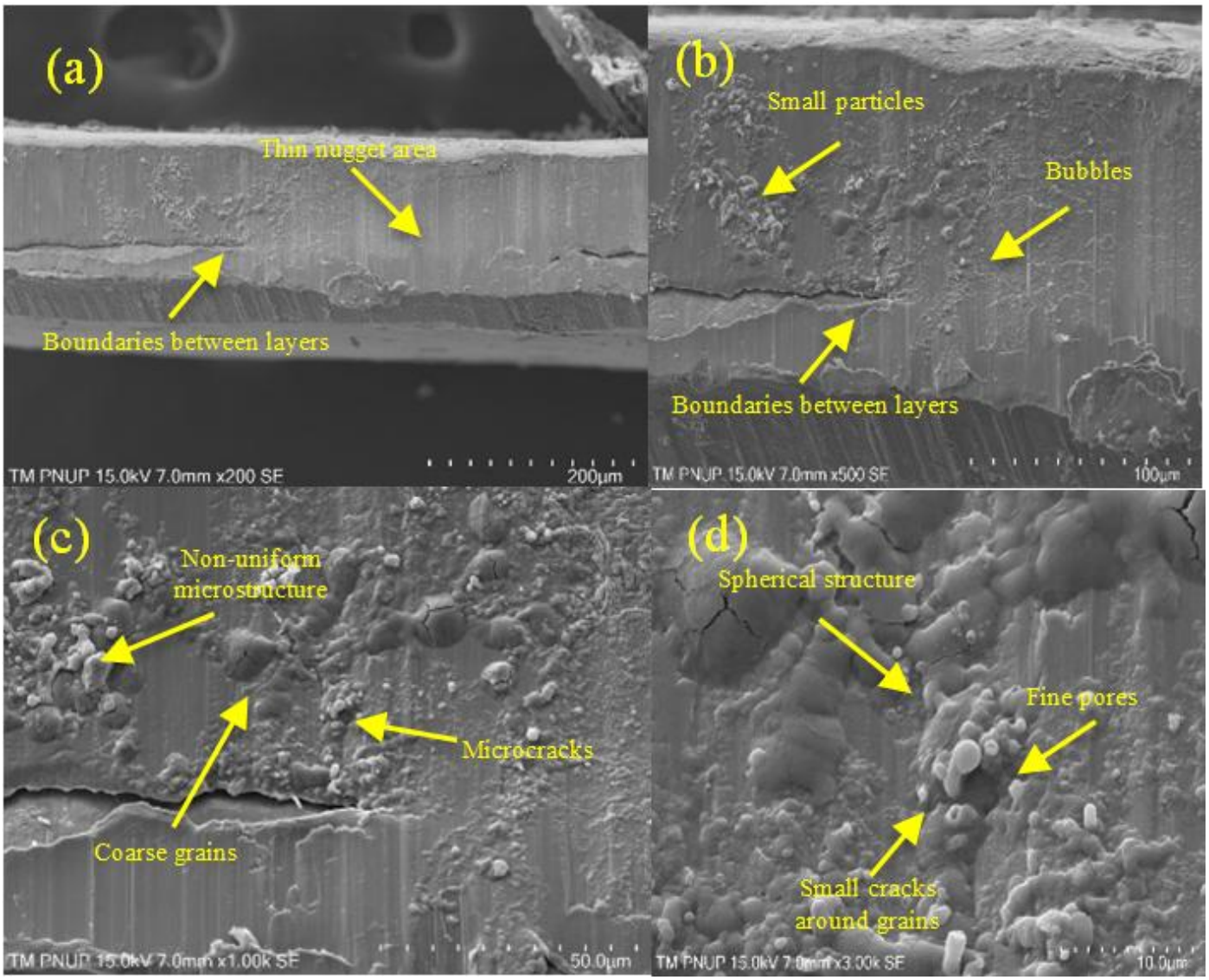

Fig. 11. SEM test results at a thickness of 0.10 mm with magnifications of (a) 200×, (b) 500×, (c) 1000×, and (d) 3000×.

Based on Fig. 11, the results of a SEM at a thickness of 0.10 mm were carried out with various magnifications of 200×, 500×, 1000×, and 3000×. At 200×, a thin nugget area is visible with the boundaries between layers still clearly visible, indicating that the welding heat has not been completely distributed, and the melting process is not optimal. 500× magnification displays a rougher surface with many small particles and bubbles due to rapid cooling, as well as the presence of a thin oxide layer that may have formed during the welding process. At 1000× magnification, a non-uniform microstructure is seen in the melting zone (fusion zone), accompanied by micro-cracks and coarse grains indicating residual stress and uneven cooling. Meanwhile, at a height of 3000×, the surface appears increasingly inhomogeneous with the appearance of spherical structures and fine pores, as well as several small cracks around the grains indicating an unstable and brittle melting area. Then the results of the EDS can be seen in the Fig. 12, in accordance with earlier findings on resistance spot welding of lithium-ion battery tabs, which reported that insufficient heat input in thin nickel tabs leads to non-uniform fusion zones, micro-crack formation, surface porosity, and localized oxidation due to rapid cooling and unstable thermal gradients [4], [5], [8]. From Fig. 12, a line analysis graphic image of a nickel spot weld joint at a thickness of 0.10 mm (Table 9).

Fig. 13 shows the process of EDS line analysis. The results of Energy Dispersive Spectroscopy (EDS) in the same area show the dominant elements of Fe (66.6 wt%), Ni (11.8 wt%), and Nb (10.7 wt%), with the presence of light elements such as C (8.1 wt%) and O (0.9 wt%). The high Fe content indicates the contribution of the base metal while Ni and Nb indicate the diffusion of coating metal and intermetallic alloys in the weld zone. Unlike C and O, it is most likely derived from the oxide layer or surface contamination due to the rapid combustion process, strengthening the existing body of evidence on resistance spot welding of lithium-ion battery tabs, which reported that EDS line analysis typically reveals Fe-

dominated regions from the base material accompanied by Ni-rich diffusion zones, while minor C and O contents are commonly associated with surface oxidation and contamination during rapid thermal cycles [1], [5].

Table 9. Line analysis results of nickel spot welding joints at a thickness of 0.10 mm

Element	Atomic %	Weight %
C (Carbon)	29.4	8.1
O (Oxygen)	2.6	0.9
F (Fluorine)	1.0	0.4
AI (Aluminum)	0.9	0.5
Fe (Iron)	51.8	66.6
Co (Cobalt)	0.5	0.7
Ni (Nickel)	8.7	11.8
Nb (Niobium)	5.0	10.7
At (Astatine)	0.0	0.0

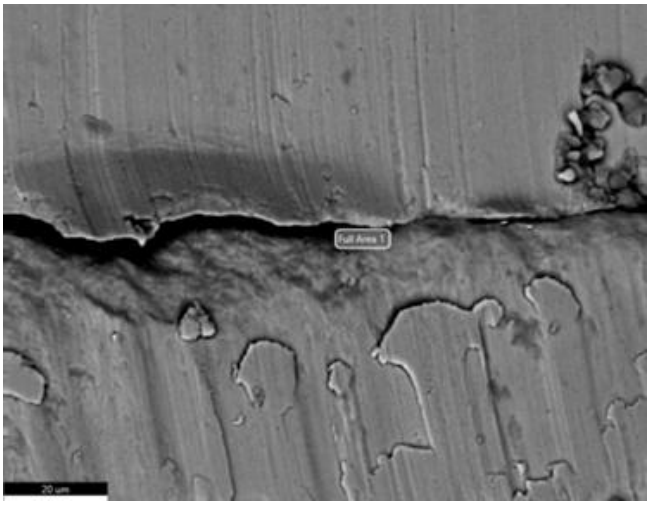

Fig. 12. EDS results 0.10 mm.

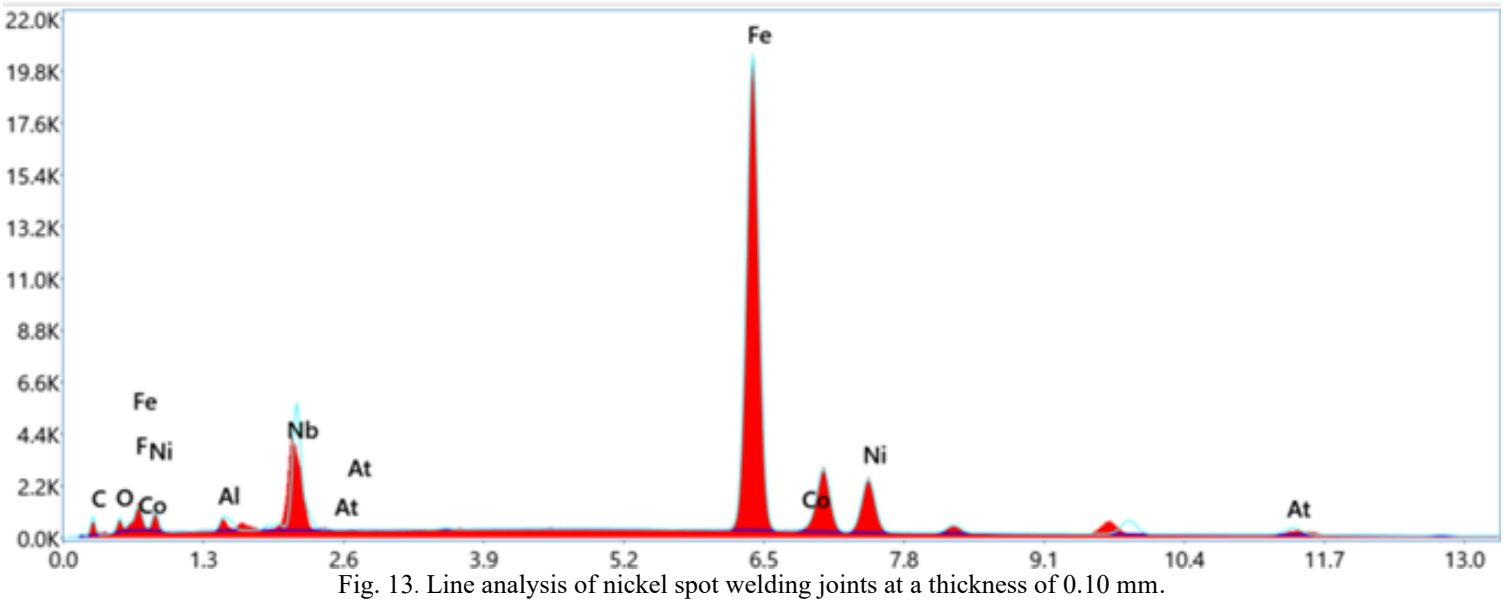

Fig. 13. Line analysis of nickel spot welding joints at a thickness of 0.10 mm.

Based on Fig. 14, the results of a SEM at a thickness of 0.10 mm were carried out with variations in magnification of 200×, 500×, 1000×, and 3000×. At a thickness of 0.12 mm, SEM observations at 200×, 500×, 1000×, and 3000× showed a relatively tighter and more homogeneous joint morphology compared to 0.10 mm. At 200×, the nugget surface appeared flatter, and the interlayer fusion was better, although there were still thin areas that had not yet merged. At 500×, clumps of particles and peeled pieces were seen along the melting boundary, which probably occurred due to partial melting and residual coating material. At 1000×, the layered structure and several small micro-cracks were clearly visible, but the number was less than at 0.10 mm; at 3,000×, small fragments and micro-pores were visible in the peeled area, indicating the presence of trapped particles and rapid local cooling, reinforcing trends reported in earlier studies on resistance spot welding of lithium-ion battery tabs, which reported that intermediate nickel thickness promotes more homogeneous fusion and improved nugget morphology compared to thinner tabs, while localized particle agglomeration, partial melting, and minor micro-cracks may still occur due to residual coating material and rapid local cooling [4], [10].

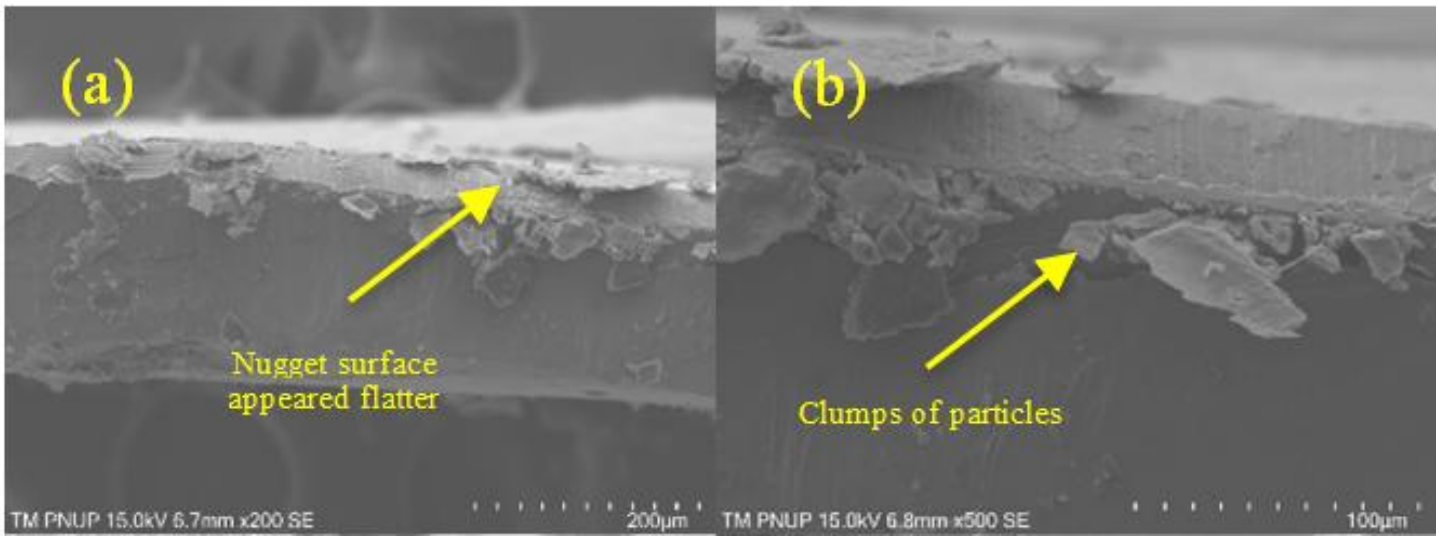

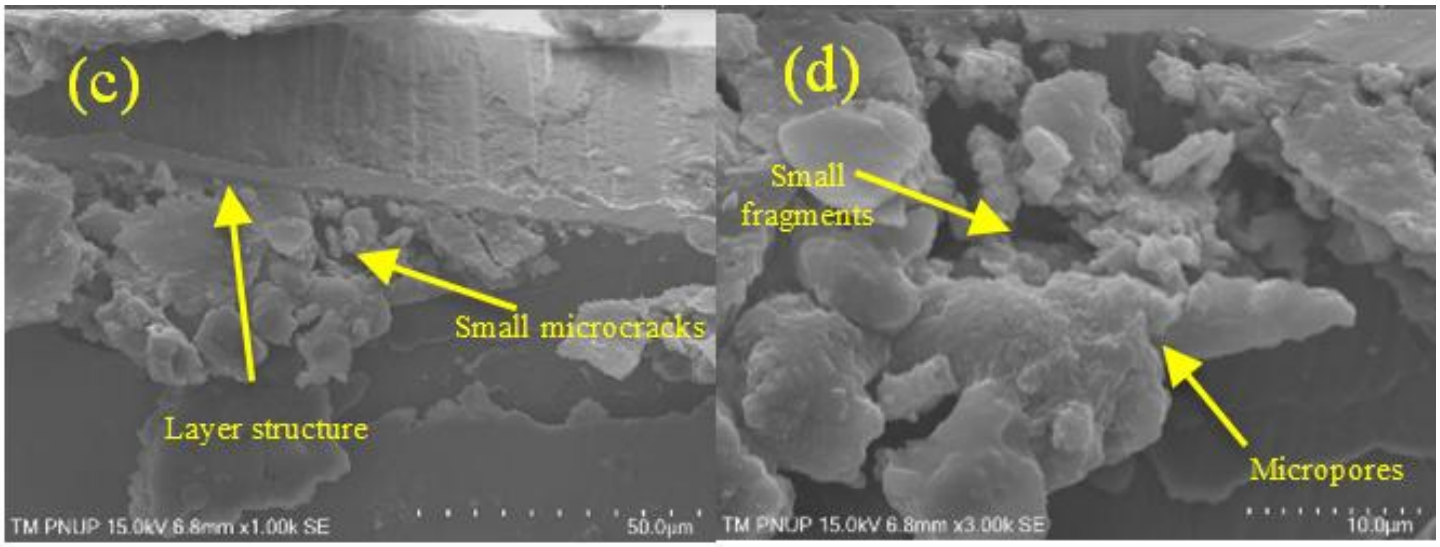

Fig. 14. SEM test results at a thickness of 0.12 mm with magnifications of (a) 200×, (b) 500×, (c) 1000×, and (d) 3000×.

From Fig. 15, a line analysis graphic image of a nickel spot weld joint at a thickness of 0.12 mm (Table 10).

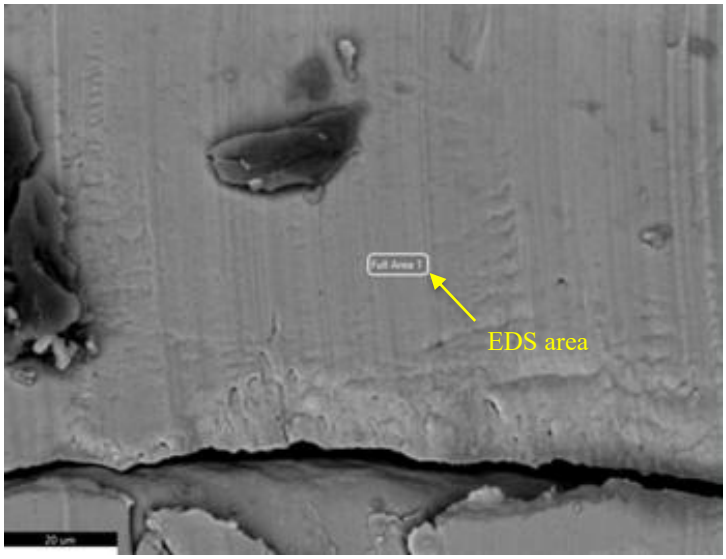

Fig. 15. EDS results at a thickness of 0.12 mm.

Table 10. Line analysis results of nickel spot welding joints at a thickness of 0.12 mm

Element	Atomic %	Weight %
C (Carbon)	35.0	10.6
O (Oxygen)	1.2	0.5
F (Fluorine)	1.1	0.5
AI (Aluminum)	0.6	0.4
Fe (Iron)	54.1	75.9
Co (Cobalt)	0.5	0.7
Ni (Nickel)	7.0	10.4
Rb (Rubidium)	0.4	0.9

Fig. 16 shows the process of EDS line analysis. The resulting spectrum image was then converted to line analysis, and several elements were detected, as listed in Table 10. This indicates a more stable Ni element and more controlled oxidation due to reduced oxygen, thus reducing visible defects in the SEM, further substantiating earlier reports on resistance spot welding of lithium-ion battery tabs, which reported that improved heat balance in intermediate nickel thickness promotes more stable Ni distribution and reduced oxygen content, leading to more controlled oxidation and fewer surface defects [4], [8], [10].

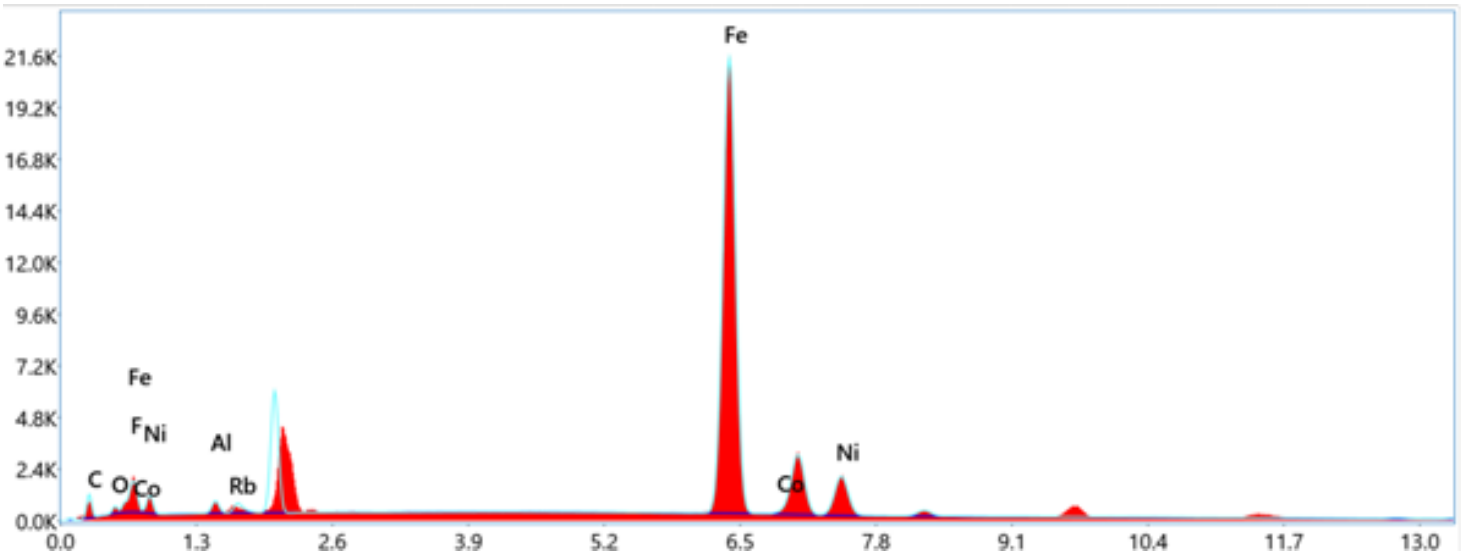

Fig. 16. Line analysis of nickel spot welding joints at a thickness of 0.12 mm.

Based on Fig. 17, it shows the results of a SEM at a thickness of 0.15 mm. At a thickness of 0.15 mm, SEM observations at 200×, 500×, 1000×, and 3000× show a relatively denser joint morphology in the core area but still display fragments and exfoliated particles on the surface. At 200×, a flatter nugget surface appears with a clear nugget-substrate boundary, but there are thin pieces attached to the edges. At 500×, many flat fragments and particle aggregates are seen piled up along the melting boundary. At 1000×, the surface structure is locally smoother but small gaps and porosity is found trapped under the pieces. At 3000×, fine grains and a layered texture are visible on the fragments.

Some fragments show wrinkled surfaces indicating non-uniformity or the presence of non-metallic phases, providing additional evidence for trends reported previously on resistance spot welding of lithium-ion battery tabs, which reported that thicker nickel tabs promote denser nugget formation, while excessive heat input may lead to surface fragmentation, exfoliated particles, and the formation of non-metallic phases due to localized overheating and uneven solidification [1], [4], [5], [11].

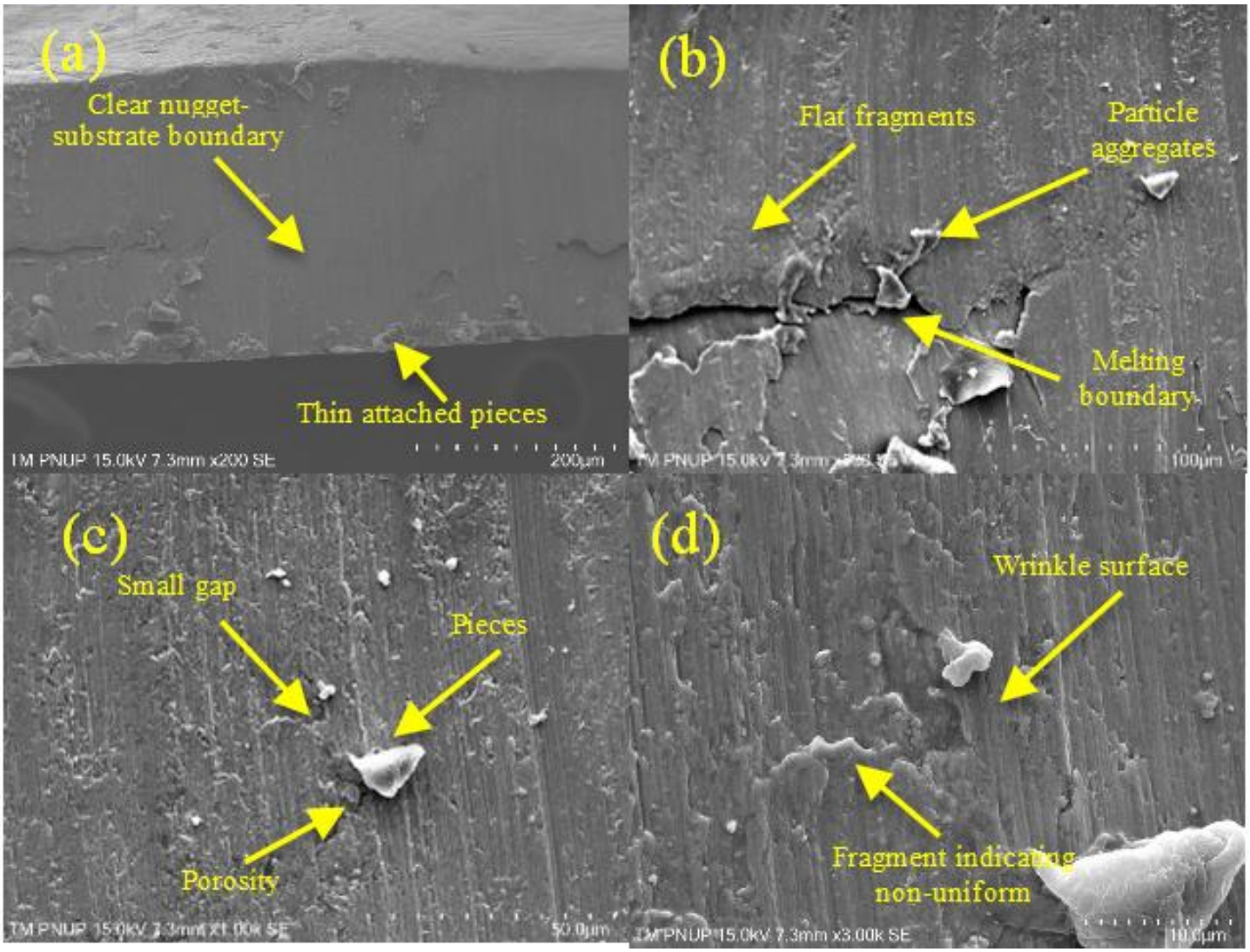

Fig. 17. SEM test results at a thickness of 0.15 mm with magnifications of (a) 200×, (b) 500×, (c) 1000×, and (d) 3000×.

From Fig. 18, a graphical image of the line analysis of the nickel spot welding joint at a thickness of 0.15 mm.

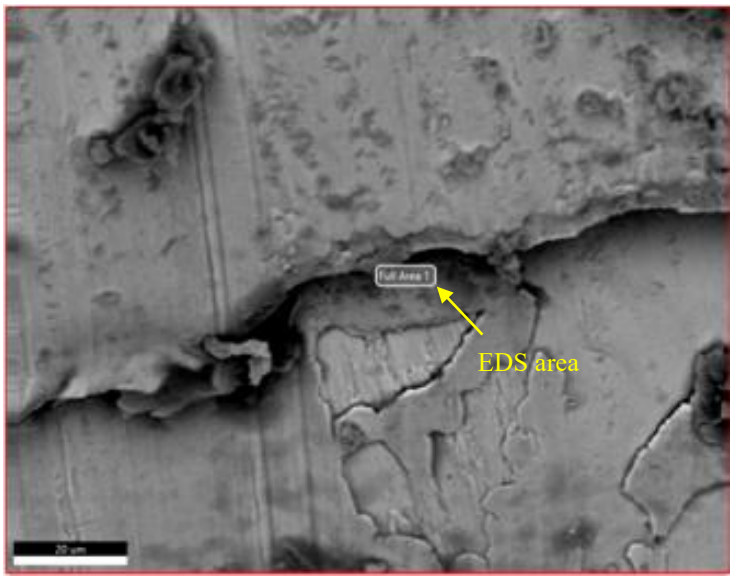

Fig. 18. EDS results at a thickness of 0.15 mm.

Fig. 19 and Table 11 show the process of EDS line analysis. In Fig. 19, the EDS results in the same area show an increase in light elements, namely C 17.4 wt% and O 3.2 wt% as well as the presence of the main metals Fe 53.9 wt%, Ni 11.8 wt%, and Nb 11.4 wt%. The high fraction of C and O can indicate the presence of surface contamination, coating residue, or oxide layers attached to the fragments, so that numerical interpretation of the metallic composition needs to be cautious and used more as a qualitative indication. Functionally, the combination of morphology (fragments/exfoliated particles and local porosity) and composition (the presence of Nb and relatively high carbon/oxides) explains why the 0.15 mm joint shows signs of good melt stability in the core area but remains susceptible to local failure in the fragment/exfoliated area.

Table 11. Line analysis results of nickel spot welding joints at a thickness of 0.15 mm

Element	Atomic %	Weight %
C (Carbon)	47.7	17.4
O (Oxygen)	6.5	3.2
F (Fluorine)	1.5	0.8
Al (Aluminum)	0.8	0.7
Si (Silicon)	1.0	0.8
K (Cobalt)	0.1	0.1
Fe (Iron)	31.8	53.9
Ni (Nickel)	6.6	11.8
Nb (Niobium)	4.0	11.4
At (Astatine)	0.0	0.0

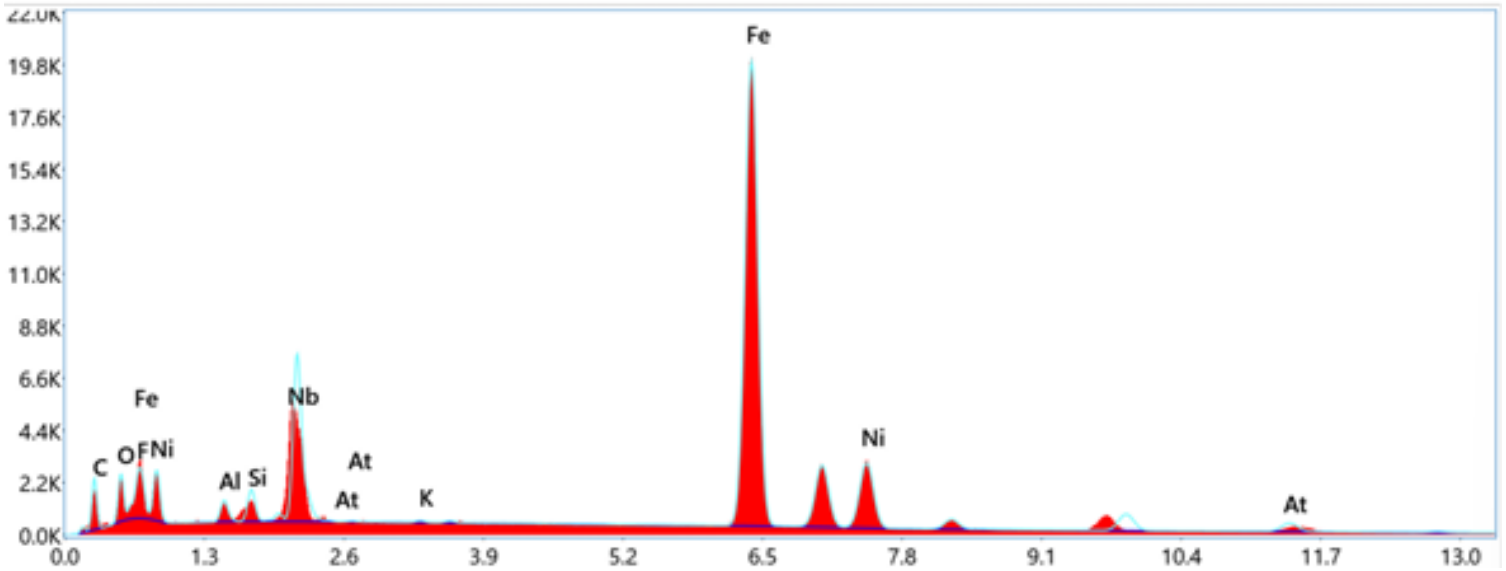

Fig. 19. Line analysis of nickel spot welding joints at a thickness of 0.15 mm.

The difference between mechanical performance and SEM–EDS observations reflects a trade-off between maximum load-bearing capacity and microstructural homogeneity. The 0.15 mm thickness provides higher load-bearing capacity due to a larger nugget formation, whereas the 0.12 mm thickness offers a more uniform microstructure due to better heat distribution, extending findings reported in prior studies on resistance spot welding of lithium-ion battery tabs, which reported a trade-off between increased nugget size and load-bearing capacity in thicker tabs and reduced microstructural homogeneity due to localized overheating, surface fragmentation, and oxide or carbonaceous residue formation [7], [8], [11].

Capacity and microstructural homogeneity in resistance spot welded nickel battery tabs. While thicker tabs maximize mechanical strength through larger nugget formation, intermediate thickness provides a more balanced heat distribution, yielding superior microstructural stability beyond strength-focused trends reported in previous studies.

4 Conclusions

This study investigates the effect of resistance spot welding parameters on the mechanical and microstructural performance of 18650 Li-ion battery joints. Based on the experimental results, the conclusions can be drawn: (1) material thickness plays a significant role in determining joint performance. A nickel strip thickness of 0.15 mm produces the highest load-bearing capacity, achieving a maximum hear force of 2380 N and peel force of 2400 N due to improved load-bearing capacity and larger nugget formation; (2) increasing the number of welding points enhances load distribution across the joint. Six welding points consistently result in higher shear and peel forces, indicating a more robust and mechanically stable joint configuration; (3) welding current has a dominant influence on joint integrity. An optimal welding current of approximately 25 A (Mode 9) provides sufficient heat input to promote strong metallurgical bonding without inducing excessive thermal damage to the battery cell or surrounding material; (4) the highest hardness value is observed in the HAZ for the 0.15 mm thickness combined with six welding points, reaching 63.74 HV. This indicates effective thermal cycling and metallurgical strengthening associated with higher heat input and nugget stability; (5) from a microstructural perspective, SEM–EDS analysis reveals that the 0.12 mm thickness exhibits a more homogeneous and uniform surface morphology, characterized by fewer micro-cracks, reduced surface fragmentation, and more stable elemental diffusion, as indicated by the dominance of Fe (75.9 wt%) and Ni (10.4 wt%).

Therefore, parameter selection should be guided by application requirements, prioritizing mechanical robustness or microstructural uniformity accordingly. For applications where maximum load-bearing capacity is critical, a 0.15 mm nickel strip combined with six welding points and higher welding current is recommended. Conversely, applications emphasizing microstructural stability and long-term reliability may benefit from a 0.12 mm thickness due to its more uniform fusion characteristics.

Acknowledgment

This work was supported by Politeknik Negeri Ujung Pandang (PNUP) through BLU Funds under the PNUP Annual Work Plan (DIPA) 2024 (Grant No. 21/12/AL.04/2025, June 12, 2025).

References

[1] M. Masomtob, R. Sukondhasingha, J. Becker, and D. U. Sauer, “Parametric study of spot welding between li-ion battery cells and sheet metal connectors,” *Eng. J.*, vol. 21, no. 7, pp. 457–473, 2017, doi: 10.4186/ej.2017.21.7.457.

[2] A. Das, “Joining Technologies for Automotive Battery Systems Manufacturing,” *World Electr. Veh. J.*, vol. 9, no. July, p. 22, 2018, doi: 10.3390/wevj9020022.

[3] M. Masomtob *et al.*, “Automotive battery pack manufacturing – a review of battery to tab joining,” *J. Adv. Join. Process.*, vol. 21, no. November 2019, p. 100017, 2020, doi: 10.1016/j.jajp.2020.100017.

[4] A. Das, D. Li, D. Williams, and D. Greenwood, “Weldability and shear strength feasibility study for automotive electric vehicle battery tab interconnects,” *J. Brazilian Soc. Mech. Sci. Eng.*, vol. 41, no. 1, pp. 1–14, 2019, doi: 10.1007/s40430-018-1542-5.

[5] N. Kumar *et al.*, “In-depth evaluation of micro-resistance spot welding for connecting tab to 18,650 Li-ion cells for electric vehicle battery application,” *Int. J. Adv. Manuf. Technol.*, vol. 121, no. 9–10, pp. 6581–6597, 2022, doi: 10.1007/s00170-022-09775-z.

[6] M. F. R. Zwicker, M. Moghadam, W. Zhang, and C. V. Nielsen, “Automotive battery pack manufacturing – a review of battery to tab joining,” *J. Adv. Join. Process.*, vol. 1, no. November 2019, p. 100017, 2020, doi: 10.1016/j.jajp.2020.100017.

[7] G. H. Farrahi, K. R. Kashyzadeh, M. Minaei, A. Sharifpour, and S. Riazi, “Analysis of Resistance Spot Welding Process Parameters Effect on the Weld Quality of Three-steel Sheets Used in Automotive Industry: Experimental and Finite Element Simulation,” *Int. J. Eng.*, vol. 33, no. 1, pp. 148–157, 2020.

[8] V. R. Rikka *et al.*, “Tailoring micro resistance spot welding parameters for joining nickel tab to inner aluminium casing in a cylindrical lithium ion cell and its influence on the

electrochemical performance," *J. Manuf. Process.*, vol. 49, no. September 2019, pp. 463–471, 2020, doi: 10.1016/j.jmapro.2019.12.014.
[9] D. Bourgeois, J. Na, A. Tiley, L. Walker, J. Middendorf, and M. Kimchi, "Investigating performance and reliability of resistance spot welds on additively manufactured battery tabs using microscopic resolution ultrasonic imaging," *Int. J. Adv. Manuf. Technol.*, vol. 137, no. 7, pp. 3479–3487, 2025, doi: 10.1007/s00170-025-15350-z.
[10] K. Bieliszczuk and M. Zyskowska, "Selected properties of single-sided resistance spot welded joints on 18650 battery tab," *Weld. Technol. Rev.*, vol. 96, pp. 4–15, 2024, doi: 10.26628/simp.wtr.v96.1176.4-15.
[11] M. Baumann, L. Wildfeuer, S. Rohr, and M. Lienkamp, "Parameter variations within Li-Ion battery packs – Theoretical investigations and experimental quantification," *J. Energy Storage*, vol. 18, no. February, pp. 295–307, 2018, doi: 10.1016/j.est.2018.04.031.
[12] S. and I. Nawawi, "The Effect Of Friction Spot Stir Welding In Double Rivet Lap Joint Installation Of Aluminum 2024-T3 On The Strength Of Shear Tests Sehono," *J. Polimesin*, vol. 21, no. 5, pp. 488–493, 2024.
[13] H. Sujono; Novianto, "Investigation of mechanical properties and dynamic characteristics of OPEFB Fiber Composite," *J. Polimesin*, vol. 22, no. 6, pp. 600–604, 2024.